FRONTIERS OF PHYSICS

RESEARCH ARTICLE
Volume 18 / Issue 2 / 23303 / 2023

Structural screening of phosphorus sulfur ternary hydride PSH_6 with a high-temperature superconductivity at 130 GPa

Yu-Long Hai, He-Jin Yan, Yong-Qing Cai†

Joint Key Laboratory of the Ministry of Education, Institute of Applied Physics and Materials Engineering, University of Macau, Taipa, Macau, China
Corresponding author. E-mail: †yongqingcai@um.edu.mo
Received June 24, 2022; accepted November 3, 2022

ABSTRACT

In our study, we constructed a series of inorganic nonmetallic ternary hydrides PSH_6 by first-principles structural screening under pressure of 200 GPa. The structural stability under lower pressure are examined. Focusing on the structural stability, electronic and phonon properties, as well as the possible superconducting properties within the framework of Bardeen–Cooper–Schrieffer (BCS) theory, we show that PSH_6 with space group $Pm\bar{3}m$ possesses a superconducting transition temperature of 146 K at 130 GPa. In the pressure range of 100–200 GPa, our work suggests that the ternary phosphorus-sulfur-hydrogen would act as a promising compositional and elemental space for achieving high-temperature superconductivity.

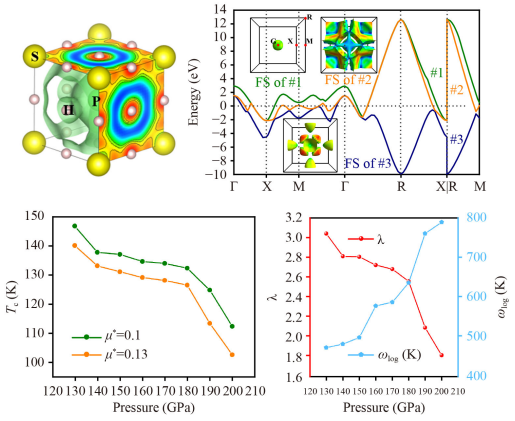

Keywords phosphoruses, sulfur, hydrides, high-temperature, superconductivity, low-pressure, structural screening

1 Introduction

Since Ashcroft put forward the concept of hydride superconductivity [1], great progress has been made in superconductivity based on hydride and its derivatives. In the prototype hydride superconductor, solid CaH_6 [2] was reported to show the T_c of 263 K at a high pressure of 200 GPa, adopting the same crystalline lattice symmetry of $Im\bar{3}m$. The highly symmetrical cubic structure makes the hydrogen atoms in this calcium hydrogen compound form a sodalite structure with H_{24}. A strong electron-phonon coupling is generated and associated with the d electrons of Ca and the highly localized hydrogen lattice. After that, the SH_3 [3] phase was found to achieve a superconducting transition temperature up to 203 K at a high pressure of 200 GPa with space group of $Im\bar{3}m$ and the ClH_3[4] has T_c under 150 GPa. In 2018, the discovery of LaH_{10} [5] and YH_{10} [5] with $Fm\bar{3}m$ showing a record-high T_c of 289 and 300 K at 200 and 250 GPa, respectively triggers ever-increasing interest in the search of novel superconducting structures in complex configurational space.

At the same time, in-depth studies of the derivative structures of these typical hydrides have also been conducted. Compared with the primitive high-pressure compound, a promoted T_c has been demonstrated through doping or substitution of LaH_{10} structure, such as TbH_{10} [6], AcH_{10} [7], $LaYH_{20}$ [8], $LaH_{9.99}B_{0.01}$ [9], KB_2H_8 [10], $LaBH_8$ [11], LaB_2H_8 [12], under an ultrahigh pressure above 200 GPa, with the charge transfer governing the superconductivity in these superconductors. For CaH_6 families, derivatives such as MgH_6 [13], $LaKH_{12}$ [14], $CaYH_{12}$ [15] and $MgCaH_{12}$ [16] were

https://doi.org/10.1007/s11467-022-1227-5

obtained under high pressure (usually 200–300 GPa), and the coupling of electrons from metallic elements and phonon from hydrogen atoms at high vibration frequencies makes the T_c of these superconductors even higher than that of their parent. In addition to above mentioned metal hydrides, high-pressure anionic hydrides based on sulfur [17], selenium [18], phosphorus [19], chloride [20] and their mixtures [21–23] have also been investigated to show a high T_c. In such compounds, the focus is on building supercells large enough to replace the target atoms in them to study the effects of doping on the system, such as $H_3S_{0.925}P_{0.075}$ (280 K, 250 GPa) [24], $H_3S_{0.9375}P_{0.0625}$ (189 K, 200 GPa) [25], $H_3S_{0.5}Se_{0.5}$ (182 K, 200 GPa) [26]. However, most of these compounds can only exist and stable under ultra-high pressure above 200 GPa. Such a high-pressure of achieving the superconducting state acts as the obstacles of promising applications. Most recently, the higher superconducting critical temperature (T_c) up to 287 K has been also observed in carbonaceous sulfur hydride CH_4-SH_3 [27] at Mbar region, this finding further proves that compressed light-element compounds are potential room temperature superconductors. In addition, theorists have predicted some of these light-element compounds which can attain high-T_c superconductivity when they are compressed to Mbar region. For example, H_6SCl [28] exhibits the superconductivity with T_c 155 K at 90 GPa. Realization of any potential high-temperature superconductors under low-pressure or even ambient pressure is of ever-evolving interests and increasingly sought-out field in condensed matter physics.

In our study, we demonstrate the realization of superconductivity in anionic compounds comprising of phosphorus, sulfur, and hydrogen atoms. Through structural exploration of the energetics of phase space, we constructed a series of inorganic nonmetallic ternary hydrides below 200 GPa. We explore a promising superconductor of PSH_6 that can work and exist in moderate pressure environment. The structural stability, electronic and phonon properties, as well as the possible superconducting properties of PSH_6 were considered within the framework of BCS theory [29]. Our results show that the PSH_6 with space group of $Pm\bar{3}m$ can reach the superconducting transition temperature of 146 K under the pressure of 130 GPa. In the pressure range of 100–200 GPa, as far as we know, there are some ternary hydrides with showing superconducting behaviors. For instance, critical superconducting transition of $BaReH_9$ (7 K, 100 GPa) [30], Li_5MoH_{11} (6.5 K, 160 GPa) [32] and CH_4-SH_3 (287 K, 267 GPa) [27] were experimentally observed. Theoretical predictions such as $MgCH_4$ (121 K, 105 GPa) [31], $MgVH_6$ (26.7 K, 150 GPa) [33], $ScYH_6$ (52.9 K, 200 GPa) [34], $LiPH_6$ (150 K, 200 GPa) [35], and LiP_2H_{14}(169 K, 230 GPa) [36] show that ternary hydrides are very promising for achieving high temperature superconductivity.

2 Computational details

In this study, the Perdew–Burke–Ernzerhof (PBE) [37] method in the Generalized Gradient Approximation (GGA) in the density functional theory [38] and the projection enhanced wave pseudopotential (PAW) [39] were adopted for the structural screening and optimization by using the VASP package [40]. A plane wave cut-off energy of 600 eV, and the k-point of the Brillouin zone was 0.01 Å^{-1} interval distribution of Monkhorst–Pack [41] for the optimization of structures, and the k-point interval of the total energy self-consistent calculation was 0.01 Å^{-1} or better. The threshold of energy convergence and force convergence were set to 10^{-5} eV and 10^{-3} eV/Å, respectively. In addition, we used Car and Perrinello [42] molecular dynamics with a $4 \times 4 \times 4$ supercell containing 512 atoms and NVT ensemble at constant temperature and pressure, and Nosé–Hoover thermostat [43] to ensure that the ambient temperature is controlled at the set value.

To investigate the dynamic stability and possible superconductivity of these cage compounds, the QUANTUM ESPRESSO package (QE) [44, 45] with the approach of density functional perturbation theory (DFPT) and PBE-GGA functional was adopted. The typical value of Coulomb pseudopotential μ^* was set as 0.1 for hydrides. Vanderbilt-type ultrasoft pseudopotentials [46] for P, S, and H were employed in this calculation. A k-mesh of $32 \times 32 \times 32$ was used in the calculation of the electron–phonon interaction matrix element and a q-mesh of $8 \times 8 \times 8$ was used for the phonon spectra calculation. The cut-off energies for the wave function and charge density are 80 Ry and 600 Ry, respectively. At the same time, the forces and stresses of the convergent structure were optimized and controlled within the error range of VASP [40] and QE [44, 45] programs.

We calculated the phonon frequency (ω) and the Eliashberg electron–phonon spectral function [$\alpha^2F(\omega)$]. Based on $\alpha^2F(\omega)$, the electron-phonon coupling constant (λ, EPC) was calculated, which is defined by integration over the entire frequency domain of $\alpha^2F(\omega)$:

$$\lambda = 2\int_0^\infty \frac{\alpha^2F(\omega)}{\omega}\mathrm{d}\omega. \quad (1)$$

For $\lambda < 1.5$, T_c was estimated by the McMillan equation [47], expressed as

$$T_c = \frac{\omega_{\log}}{1.2}\exp\left[-\frac{1.04(1+\lambda)}{\lambda-\mu^*(1+0.62\lambda)}\right]. \quad (2)$$

The EPC parameter λ is larger than 1.5, which represents very strong electron–phonon coupling for systems. T_c was corrected by Allen–Dynes–corrected McMillan equation [48], expressed as

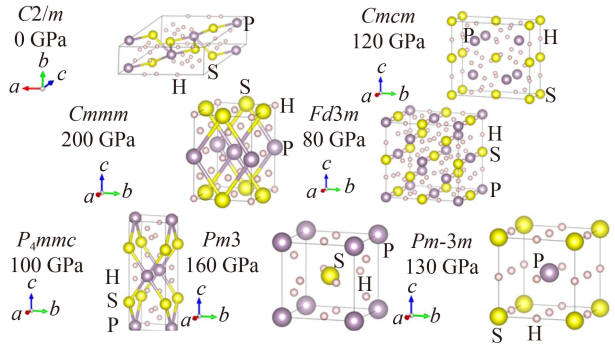

Fig. 1 Intermediate polymorph structures of phosphorus-sulfur-hydrogen (PSH_6) ternary compounds at various pressures. The gray, yellow and pink spheres represent phosphorus, sulfur and hydrogen, respectively.

$$T_c = f_1 f_2 \frac{\omega_{\log}}{1.2} \exp\left[-\frac{1.04(1+\lambda)}{\lambda - \mu^*(1+0.62\lambda)}\right], \tag{3}$$

where

$$f_1 = \left\{1 + \left[\frac{\lambda}{2.46(1+3.8\mu^*)}\right]^{3/2}\right\}^{1/3}, \tag{4}$$

$$f_2 = 1 + \frac{\lambda^2(\omega/\omega_{\log} - 1)}{\lambda^2 + [1.82(1+6.3\mu^*)(\omega/\omega_{\log})]^2} \tag{5}$$

are the correction factors. $\omega_{\log}$ is the logarithmic average of phonon frequency and is written as

$$\omega_{\log} = \exp\left[\frac{2}{\lambda}\int_0^\infty \frac{\alpha^2 F(\omega)\log(\omega)}{\omega} d\omega\right]. \tag{6}$$

In electron part and electron–phonon parts, we use "Methfessel–Paxton first-order spreading" method [49] and the value of the Gaussian spreading for Brillouin-zone integration was set to 0.01 Ry.

3 Results and discussion

We have screened more than 10000 crystal structures composed of phosphorus, sulfur and hydrogen based on particle swarm optimization (PSO) method using CALYPSO code [50–52], and the results are summarized in Fig. S1 of the Supplemental Material. Among these ternary compounds, three compounds PSH_3, PSH_6 and PSH_8 were found to be thermodynamically stable. Among them, the PSH_6 has superconducting properties with superconducting transition T_c of more than 140 K. Although PSH_3 and PSH_8 also have a good thermal stability, unfortunately, we cannot find low-pressure polymorph of them with promising superconducting phases. Next, we would like to focus on PSH_6 and explore its intermediate structures under varying pressure.

By using CALYPSO [50–52], we successfully identified

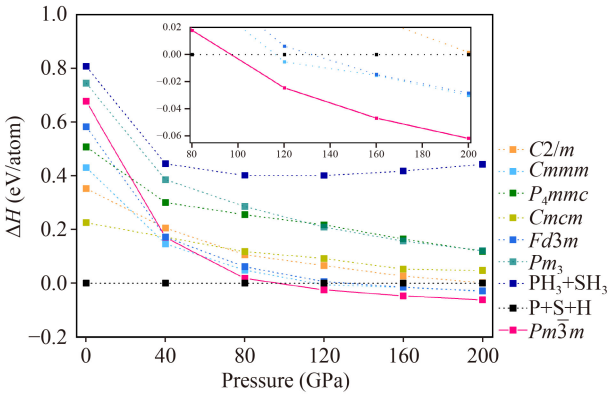

Fig. 2 Relative formation enthalpy of various high-symmetry phases of PSH_6 with pressure in the range of 0 – 200 GPa.

more than 1000 structures of PSH_6 under different pressure conditions, suggesting the existence of rich polymorphs of this ternary compound.Amongst the various intermediate structures (Fig. 1), we obtained a structure of $Pm\bar{3}m$ showing intriguing superconducting properties with the T_c occurring at relatively low pressure. As shown in Fig. 1, in the novel $Pm\bar{3}m$ phase of PSH_6 the phosphorus atom is located at the body center of the lattice, and the fractional Cartesian coordinate is (0.5, 0.5,0.5), and the sulfur atom occupies lattice vertices, and the Cartesian coordinate is (0,0,0). Six hydrogen atoms occupy the face centers and middle edges, respectively.

As shown in Fig. 2, we plotted formation enthalpy of PSH_6 at different pressures. Here the enthalpy of formation process of gaseous P + S + H is used as the reference. We found that the $C2/m$, P_4mmc, $Cmcm$, Pm_3 and PH_3+SH_3 structures are significantly higher than that of P + S + H at the pressure range of 0–200 GPa. This suggests that a thermodynamic stability of these polymorph at the pressure is worse than that of P + S + H, implying a phase decomposition into gaseous elements. Similarly, at the pressure range of 98–200 GPa, as shown in the inset of Fig. 2, the $Pm\bar{3}m$ phase is the most thermodynamically stable structure among the existing candidates. Further, we also considered the possibility of the decomposition of PSH_6 into other stable binary compounds (as marked in Fig. S1), such as $2PH_3 + 2SH_2 + H_2$, $P_2S_7 + 5PH_3 + 27/2H_2$, $P_2S_5 + 3PH_3 + 21/2H_2$, $P_4S_7 + 3PH_3 + H_2$, $P_4S_9 + 5PH_3 + 39/2H_2$ and $P_4S_3 + SH_3 + 21/2H_2$. These results are presented in Fig. S3 of the Supplemental Material, indicating that PSH_6 will not decompose into the similar products at above pressures. Therefore, the PSH_6 is prone to be thermodynamically stable between 98–200 GPa.

In order to further evaluate the structural stability of $Pm\bar{3}m$ phase of the PSH_6, we examine its structural stability at the dual effects of pressure and temperature from the perspective of molecular dynamics. At applying a pressure of 130 GPa, the structure was simulated with

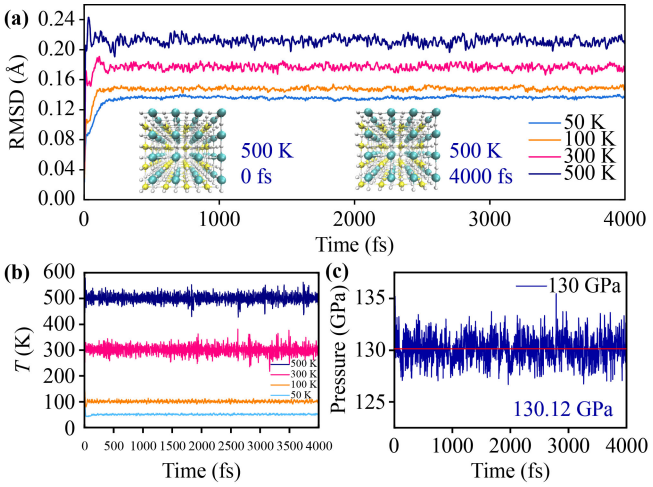

Fig. 3 **(a)** RMSD of $Pm\bar{3}m$ PSH_6 simulated by the ab-initio molecular dynamics at 130 GPa and at temperatures between 50–500 K; **(b)** Time-temperature profiles at a series of temperatures; **(c)** Oscillation of pressure set at 130 GPa.

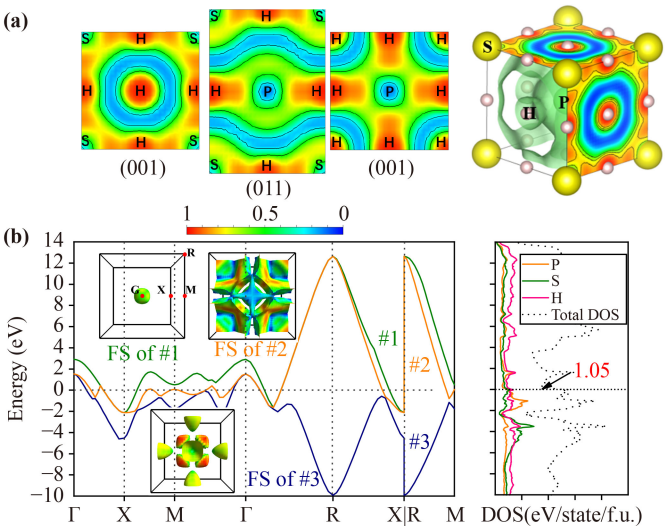

Fig. 4 **(a)** Electronic local function (ELF) of $Pm\bar{3}m$ PSH_6 at 130 GPa; **(b)** Band structure of and DOS (right) of $Pm\bar{3}m$ PSH_6 at 130 GPa. The insets show the Fermi surfaces of band 1, 2 and 3.

ab initio molecular dynamics at a series temperatures of 50,100,200,300 and 500 K. The detailed relaxation process at different temperatures is shown in Fig. 3(a). We calculated the root-mean-square displacement (RMSD) of PSH_6 at 50,100,300 and 500 K which are found to be 0.135, 0.147, 0.176 and 0.211 Å, respectively. As expected, the actual temperature of the thermostat fluctuates near the set values, as shown in Fig. 3(b). The steady evolution around the targeted temperature signifies a robust structure of the PSH_6 phase without any abrupt collapse of structure nor bond breaking at disturbances of thermal and stress. Similarly, as shown in Fig. 3(c), the in-situ pressure is overall maintained around 130 GPa which also excludes the discontinuity associated with any structural reconstruction. Therefore, at the pressure of 130 GPa and the temperature of 50–500 K, the PSH_6 still maintains the stability and integrity of the structure. We also considered higher pressures up to 200 GPa, the atomic RMSD for temperatures between 50–500 K is similar to that in 130 GPa, as shown in Fig. S4 of the Supplemental Material. Therefore, the PSH_6 phase still maintains a dynamic stability at broad windows of pressure and temperature.

Based on above analysis from thermodynamics and structural dynamics, we can safely conclude that the novel $Pm\bar{3}m$ phase of PSH_6 will not be decomposed at the condition of 98–200 GPa, and can still maintain the stability of the structure at the condition of 98–200 GPa. This sets a solid foundation of exploring its superconducting properties.

After confirming that the $Pm\bar{3}m$ PSH_6 can stably exist at certain pressures, we next focus on the electronic structure of this phosphorus-sulfur-hydrogen compound. The ternary compound can be regarded as a cubic structure formed by the nesting of PH_3 and SH_3 in space, which is also confirmed by the electronic local function (ELF) as shown in Fig. 4(a). Owing to a stronger electronegativity, the sulfur atoms tend to attract more electrons from hydrogens, which is proved by bader charge analysis. Each S and P atom get 0.189 and 0.177 electrons respectively, while the H atom around the S (P) atom loses 0.119 (0.004) electron. Therefore more electrons are localized around the S atom. From the ELF, it is found that there is stronger polar bond between S and H than between P and H, which is because S has stronger electronegativity than P. Compared with S atom, there are fewer electrons localized around P atom, indicating that the electrons of H tend to be distributed at the joint region between H and P atoms.

Band structure around the Fermi level is plotted in Fig. 4(b). A good metallicity is found for the $Pm\bar{3}m$ PSH_6 phase as reflected by the partially occupied bands crossing the Fermi level. Another feature of the electronic band structure is the rich distribution of valleys, for instance, the electron pockets along the X–M–Γ path. Here different colors are used to differentiate each band crossing the Fermi energy, as shown in Fig. 4(b). The Fermi surface corresponding to each band is plotted in the inset, from which the pocket states exist around the zone center and high symmetrical sites at face centers and corners. The projected electronic density of states (DOS) of PSH_6 are shown in Fig. 4(b). At the Fermi level, the P, S, and H contribute roughly equally and lead to a robust metallicity. This is quite surprising as H only having one valence electron and the evenly distributed H states spread over the whole energy range. In real space, those H atoms at edge and face centers form hybridized states with S and P in form of conducting channels along the cubic edge connecting the vertices (S

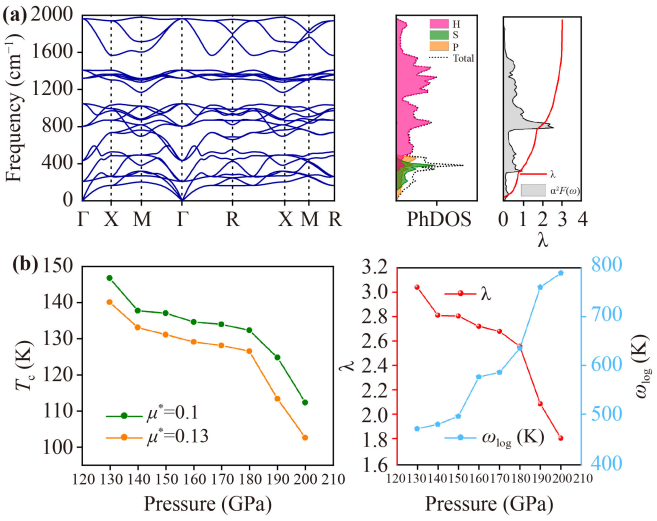

Fig. 5 **(a)** Phonon spectrum, phonon density of states (PhDOS), and Eliashberg spectrum function $\alpha^2F(\omega)$, and electron-phonon coupling integral $\lambda(\omega)$ of PSH_6 at 130 GPa. **(b)** Pressure dependence of T_c, λ, and ω_{log} of PSH_6.

atom) and cubic center (P atom).

Finally, we would like to show the possible aspect of achieving superconduction and its related mechanism of PSH_6. As shown in Fig. 5(a), the frequency range of phonon vibration is 0–2000 cm^{-1}. Among them, the high- and middle-frequency vibrational modes (more than 600 cm^{-1}) are mainly associated with the vibration of hydrogen atoms, while the low-frequency vibration at 0–600 cm^{-1} mainly involves with the vibration of phosphorus and sulfur atoms with a minor contribution of hydrogen. By integrating the Eliashberg function, we can obtain the electron-phonon coupling constant λ. In the low frequency part, mainly contributed by the heavier phosphorus and sulfur atoms, the growth rate of λ is slow but steady. In the high-frequency region with vibrations dominated by hydrogen, the λ grows quickly and finally saturates to 3.02, comparably contributed by the hydrogen and phosphorus and sulfur, and which is larger than 2.19 of H_3S at 200 GPa.

The variation of superconducting transition temperature T_c with pressure is shown in Fig. 5(b). At 130 GPa, when $\mu^\star$ is 0.1 and 0.13 the T_c is 146.5 K and 139.9 K, respectively. In a similar pressure range, as far as we know, there is no inorganic nonmetallic ternary hydrides with T_c higher than PSH_6. We found that the T_c decreases with the increase of pressure. When the pressure increases to 200 GPa, T_c is reduced to 112.13–102.44 K. The λ has a similar trend with the increase of pressure, while the ω_{log} shows the opposite trend [Fig. 5(b) right].

Unfortunately, although other structures can be metallized at pressure, it is less likely to be promising for superconducting due to the unstable phonon structures.

4 Conclusion

In summary, via screening the energy landscapes of the P–S–H ternary phase space at pressure, we have identified and explored a metastable phase of PSH_6 with respect to its structural stability (thermodynamic stability and dynamic stability), electronic structure, phonon structure and superconducting properties. We found that the $Pm\bar{3}m$ structure reveals a good metallicity, stable phonon dispersions, and a relatively high superconducting transition temperatures of 146 K at a moderate pressure of 130 GPa. The discovery of PSH_6 superconductivity suggests that the P–S–H systems are promising for the exploration of relatively low-pressure and high-temperature superconductors.

Electronic supplementary material Supplementary materials are available in the online version of this article at https://doi.org/10.1007/s11467-022-1227-5 and https://journal.hep.com.cn/fop/EN/10.1007/s11467-022-1227-5 and are accessible for authorized users.

Ackonwledgements This work was supported by the National Natural Science Foundation of China (Grant 22022309), and the Natural Science Foundation of Guangdong Province, China (2021A1515010024), the University of Macau (SRG2019-00179-IAPME, MYRG2020-00075-IAPME), the Science and Technology Development Fund from Macau SAR (FDCT-0163/2019/A3). This work was performed at the High Performance Computing Cluster (HPCC), which is supported by the Information and Communication Technology Office (ICTO) of the University of Macau.

References

1. N. W. Ashcroft, Hydrogen dominant metallic alloys: High temperature superconductors? *Phys. Rev. Lett.* 92(18), 187002 (2004)
2. H. Wang, J. S. Tse, K. Tanaka, T. Iitaka, and Y. Ma, Superconductive sodalite-like clathrate calcium hydride at high pressures, *Proc. Natl. Acad. Sci. USA* 109(17), 6463 (2012)
3. D. Duan, Y. Liu, F. Tian, D. Li, X. Huang, Z. Zhao, H. Yu, B. Liu, W. Tian, and T. Cui, Pressure-induced metallization of dense $(H_2S)_2H_2$ with high-T_c superconductivity, *Sci. Rep.* 4(1), 6968 (2015)
4. A. P. Durajski and R. Szczesniak, Structural, electronic, vibrational, and superconducting properties of hydrogenated chlorine, *J. Chem. Phys.* 149(7), 074101 (2018)
5. H. Liu, I. I. Naumov, R. Hoffmann, N. W. Ashcroft, and R. J. Hemley, Potential high-T_c superconducting lanthanum and yttrium hydrides at high pressure, *Proc. Natl. Acad. Sci. USA* 114(27), 6990 (2017)
6. Y. L. Hai, N. Lu, H. L. Tian, M. J. Jiang, W. Yang, W. J. Li, X. W. Yan, C. Zhang, X. J. Chen, and G. H. Zhong, Cage structure and near room-temperature superconductivity in TbH_n (n = 1–12), *J. Phys. Chem. C* 125(6), 3640 (2021)
7. D. V. Semenok, A. G. Kvashnin, I. A. Kruglov, and A.

R. Oganov, Actinium hydrides AcH_{10}, AcH_{12}, and AcH_{16} as high-temperature conventional superconductors, *J. Phys. Chem. Lett.* 9(8), 1920 (2018)
8. D. V. Semenok, I. A. Troyan, A. G. Ivanova, A. G. Kvashnin, I. A. Kruglov, M. Hanfland, A. V. Sadakov, O. A. Sobolevskiy, K. S. Pervakov, I. S. Lyubutin, K. V. Glazyrin, N. Giordano, D. N. Karimov, A. L. Vasiliev, R. Akashi, V. M. Pudalov, and A. R. Oganov, Superconductivity at 253 K in lanthanum–yttrium ternary hydrides, *Mater. Today* 48, 18 (2021)
9. Y. Ge, F. Zhang, and R. J. Hemley, Room-temperature superconductivity in boron-nitrogen doped lanthanum superhydride, arXiv: 2012.13398 (2020)
10. M. Gao, X. W. Yan, Z. Y. Lu, and T. Xiang, Phonon-mediated high-temperature superconductivity in the ternary borohydride KB_2H_8 under pressure near 12 GPa, *Phys. Rev. B* 104(10), L100504 (2021)
11. S. Di Cataldo, C. Heil, W. von der Linden, and L. Boeri, $LaBH_8$: Towards high-T_c low-pressure superconductivity in ternary superhydrides, *Phys. Rev. B* 104(2), L020511 (2021)
12. X. W. Liang, A. Bergara, X. D. Wei, L. Y. Wang, R. X. Sun, H. Y. Liu, R. J. Hemley, L. Wang, G. Y. Gao, and Y. J. Tian, Prediction of high-T_c superconductivity in ternary lanthanum borohydrides, arXiv: 2107.02553 (2021)
13. X. Feng, J. Zhang, G. Gao, H. Liu, and H. Wang, Compressed sodalite-like MgH_6 as a potential high-temperature superconductor, *RSC Advances* 5(73), 59292 (2015)
14. P. Song, Z. Hou, P. Castro, K. Nakano, K. Hongo, Y. Takano, and R. Maezono, High-T_c ternary metal hydrides, YKH_{12} and $LaKH_{12}$, discovered by machine learning, arXiv: 2103.00193 (2021)
15. X. W. Liang, A. Bergara, L. Y. Wang, B. Wen, Z. S. Zhao, X. F. Zhou, J. L. He, G. Y. Gao, and Y. J. Tian, Potential high-T_c superconductivity in $CaYH_{12}$ under pressure, *Phys. Rev. B* 99, 100505(R) (2019)
16. W. Sukmas, P. Tsuppayakorn-aek, U. Pinsook, and T. Bovorn-ratanaraks, Near-room-temperature superconductivity of Mg/Ca substituted metal hexahydride under pressure, *J. Alloys Compd.* 849, 156434 (2020)
17. C. Heil and L. Boeri, Influence of bonding on superconductivity in high-pressure hydrides, *Phys. Rev. B* 92, 060508(R) (2015)
18. D. A. Papaconstantopoulos, Possible high-temperature superconductivity in hygrogenated fluorine, *Nov. Supercond. Mater.* 3(1), 29 (2017)
19. A. P. Drozdov, M. I. Eremets, and I. A. Troyan, Superconductivity above 100 K in PH_3 at high pressures, arXiv: 1508.06224 (2015)
20. A. P. Durajski and R. Szczesniak, Structural, electronic, vibrational, and superconducting properties of hydrogenated chlorine, *J. Chem. Phys.* 149(7), 074101 (2018)
21. B. Liu, W. Cui, J. Shi, L. Zhu, J. Chen, S. Lin, R. Su, J. Ma, K. Yang, M. Xu, J. Hao, A. P. Durajski, J. Qi, Y. Li, and Y. Li, Effect of covalent bonding on the superconducting critical temperature of the H-S-Se system, *Phys. Rev. B* 98(17), 174101 (2018)
22. X. Y. Wang, T. G. Bi, K. P. Hilleke, A. Lamichhane, R. J. Hemley, and E. Zurek, A little bit of carbon can do a lot for superconductivity in H_3S, arXiv: 2109.09898 (2021)
23. Y. F. Ge, F. Zhang, R. P. Dias, R. J. Hemley, and Y. G. Yao, Hole-doped room-temperature superconductivity in $H_3S_{1-x}Z$ (Z = C, Si), *Mater. Today Phys.* 15, 100330 (2020)
24. Y. Ge, F. Zhang, and Y. Yao, First-principles demonstration of superconductivity at 280 K in hydrogen sulfide with low phosphorus substitution, *Phys. Rev. B* 93(22), 224513 (2016)
25. A. Nakanishi, T. Ishikawa, and K. Shimizu, First-principles study on superconductivity of P- and Cl-doped H_3S, *J. Phys. Soc. Jpn.* 87(12), 124711 (2018)
26. Z. J. Shao, H. Song, H. Y. Yu, and D. F. Duan, *Ab initio* investigation on the doped H_3S by V, VI, and VII group elements under high pressure, *J. Supercond. Nov. Magn.* 35(4), 979 (2022)
27. E. Snider, N. Dasenbrock-Gammon, R. McBride, M. Debessai, H. Vindana, K. Vencatasamy, K. V. Lawler, A. Salamat, and R. P. Dias, Room-temperature superconductivity in a carbonaceous sulfur hydride, *Nature* 586, 373 (2020)
28. Y. L. Hai, H. L. Tian, M. J. Jiang, H. B. Ding, Y. J. Feng, G. H. Zhong, C. L. Yang, X. J. Chen, and H. Q. Lin, Prediction of high-T_c superconductivity in H_6SX (X = Cl, Br) at pressures below one megabar, *Phys. Rev. B* 105(18), L180508 (2022)
29. J. Bardeen, L. Cooper, and J. Schrieffer, Theory of superconductivity, *Phys. Rev.* 108(5), 1175 (1957)
30. T. Muramatsu, W. K. Wanene, M. Somayazulu, E. Vinitsky, D. Chandra, T. A. Strobel, V. V. Struzhkin, and R. J. Hemley, Metallization and superconductivity in the hydrogen-rich ionic salt $BaReH_9$, *J. Phys. Chem. C* 119(32), 18007 (2015)
31. F. B. Tian, D. Li, D. F. Duan, X. J. Sha, Y. X. Liu, T. Yang, B. B. Liu, and T. Cui, Predicted structures and superconductivity of hypothetical Mg-CH_4 compounds under high pressures, *Mater. Res. Express* 2(4), 046001 (2015)
32. D. Z. Meng, M. Sakata, K. Shimizu, Y. Iijima, H. Saitoh, T. Sato, S. Takagi, and S. Orimo, Superconductivity of the hydrogen-rich metal hydride Li_5MoH_{11} under high pressure, *Phys. Rev. B* 99(2), 024508 (2019)
33. J. Zheng, W. G. Sun, X. L. Dou, A. J. Mao, and C. Lu, pressure-driven structural phase transitions and superconductivity of ternary hydride $MgVH_6$, *J. Phys. Chem. C* 125(5), 3150 (2021)
34. Y. K. Wei, L. Q. Jia, Y. Y. Fang, L. J. Wang, Z. X. Qian, J. N. Yuan, G. Selvaraj, G. F. Ji, and D. Q. Wei, Formation and superconducting properties of predicted ternary hydride $ScYH_6$ under pressures, *Int. J. Quantum Chem.* 121(4), e26459 (2020)
35. Z. J. Shao, D. F. Duan, Y. B. Ma, H. Y. Yu, H. Song, H. Xie, D. Li, F. B. Tian, B. B. Liu, and T. Cui, Ternary superconducting cophosphorus hydrides stabilized via lithium, *npj Comput. Mater.* 5, 104 (2019)
36. X. Li, Y. Xie, Y. Sun, P. H. Huang, H. Y. Liu, C. F. Chen, and Y. M. Ma, Chemically tuning stability and superconductivity of P–H compounds, *J. Phys. Chem. Lett.* 11(3), 935 (2020)
37. J. P. Perdew, K. Burke, and M. Ernzerhof, Generalized

gradient approximation made simple, *Phys. Rev. Lett.* 77(18), 3865 (1996)
38. W. Kohn and L. J. Sham, Self-consistent equations including exchange and correlation effects, *Phys. Rev.* 140(4A), A1133 (1965)
39. G. Kresse and D. Joubert, From ultrasoft pseudopotentials to the projector augmented-wave method, *Phys. Rev. B* 59(3), 1758 (1999)
40. G. Kresse and J. Furthmüller, Efficiency of *ab-initio* total energy calculations for metals and semiconductors using a plane-wave basis set, *Comput. Mater. Sci.* 6(1), 15 (1996)
41. D. J. Chadi, Special points for Brillouin-zone integrations, *Phys. Rev. B* 16(4), 1746 (1977)
42. R. Car and M. Parrinello, Unified approach for molecular dynamics and density-functional theory, *Phys. Rev. Lett.* 55(22), 2471 (1985)
43. W. G. Hoover, Canonical dynamics: Equilibrium phase-space distributions, *Phys. Rev. A* 31(3), 1695 (1985)
44. P. Giannozzi, S. Baroni, N. Bonini, M. Calandra, R. Car, et al., QUANTUM ESPRESSO: A modular and open-source software project for quantum simulations of materials, *J. Phys.: Condens. Matter* 21(39), 395502 (2009)
45. P. Giannozzi, O. Andreussi, T. Brumme, O. Bunau, M. B. Nardelli, et al., Advanced capabilities for materials modelling with QUANTUM ESPRESSO, *J. Phys.: Condens. Matter* 29(46), 465901 (2017)
46. D. Vanderbilt, Soft self-consistent pseudopotentials in a generalized eigenvalue formalism, *Phys. Rev. B* 41(11), 7892 (1990)
47. R. C. Dynes, McMillan's equation and the T_c of superconductors, *Solid State Commun.* 10(7), 615 (1972)
48. P. B. Allen and R. C. Dynes, Transition temperature of strong-coupled superconductors reanalyzed, *Phys. Rev. B* 12(3), 905 (1975)
49. M. Methfessel and A. T. Paxton, High-precision sampling for Brillouin-zone integration in metals, *Phys. Rev. B* 40(6), 3616 (1989)
50. Y. Wang, J. Lv, L. Zhu, and Y. Ma, CALYPSO: A method for crystal structure prediction, *Comput. Phys. Commun.* 183(10), 2063 (2012)
51. B. Gao, P. Gao, S. Lu, J. Lv, Y. Wang, and Y. Ma, Interface structure prediction via CALYPSO method, *Sci. Bull. (Beijing)* 301, 64 (2019)
52. P. Y. Gao, B. Gao, S. H. Lu, H. Y. Liu, J. Lv, Y. C. Wang, and Y. M. Ma, Structure search of two-dimensional systems using CALYPSO methodology, *Front. Phys.* 17(2), 23203 (2022)